CHAPTER 6

Synthesis of solketal using transition metal-based acid catalyst

6.1 Introduction

The rise in global biodiesel production leads to the surplus of glycerol as a byproduct, necessitating its industrial application in various chemicals to sustain the biodiesel industry economically. Solketal is one of the valuable value-added chemicals in the biodiesel industry, with numerous applications in the food, polymer, and chemical industries and fuel additives. Nowadays, researchers mainly focus on synthesizing solketal using biowaste glycerol coming from the biodiesel industry due to its immense applications. In this work, the experimental data demonstrated that incorporating $ZnAl_2O_4$ played a key role in establishing the surface sulfate groups and the structural composite of the solid acid catalyst. Highly efficient heterogeneous acid $SO_4^{2-}/ZnAl_2O_4$-ZrO_2 and $SO_4^{2-}/ZnAl_2O_4$-TiO_2 catalysts were synthesized and applied for solketal synthesis. It was found that SZZ proved to be highly efficient and active towards glycerol conversion of 99.3 % with 98 % solketal yield. In contrast, SZT shows 83 % glycerol conversion with 81 % solketal yield at the optimized reaction conditions. SZZ showed excellent catalytic activity compared to SZT due to its better reusability, higher acidity, and good structural stability. Green metrics parameters like E-factor, PMI, and AE were performed, and it found that SZZ is more efficient and the acetalization reaction of glycerol is environmentally friendly in nature.

6.2 Catalyst synthesis process

The coprecipitation and wet impregnation techniques were utilized in the synthesis of solid acid heterogeneous catalysts, specifically $SO_4^{2-}/ZnAl_2O_4$-ZrO_2 and $SO_4^{2-}/ZnAl_2O_4$-TiO_2 named SZZ and SZT respectively. At first, $ZnAl_2O_4$ was synthesized by the co-precipitation process using nitrate salt as a precursor. In this procedure, the required quantity of zinc nitrate and aluminum nitrate was taken and dissolved in deionized water separately (Zn: Al is 1:2). At 30 ^oC, both the solutions were mixed and stirred for 3-4 h.

with the adding ammonium hydroxide solution drop by drop to regulate the solution's pH within the range of 8-10. The resulting solution mixture was agitated additionally for 5-6 h. to promote selective precipitation growth. Following filtration, the reaction mixture was rinsed with distilled water three to four times to eliminate any remaining impurities. The solid mixture was then placed in a hot air oven at 120 ^{o}C for 8 h. and subsequentially calcined at 700 ^{o}C for 5 h. in an air muffle furnace to get the desired spinel. Then, the stipulated amount of $ZnAl_2O_4$ was immersed in deionized water and added to ZrO_2. In order to augment the acidic strength of the synthesized catalyst, the mixture powder was emersed with 0.5M H_2SO_4 for 5-6 h. at 550 rpm by wetness impregnation. Afterward, the white powder underwent heat treatment in an oven overnight at 90 ^{o}C and was then calcined at 550 ^{o}C in an air muffle furnace for intervals of 3 h intervals with a 10 ^{o}C/min heating rate to get $SO_4^{2-}/ZnAl_2O_4$-ZrO_2. Finally, the calcined catalyst was ground with mortar and pestle, stored in a desiccator to prevent moisture, and further applied for the acetalization reaction. Another acetalization catalyst, like $SO_4^{2-}/ZnAl_2O_4$-TiO_2, was also created and tested similarly, as discussed above.

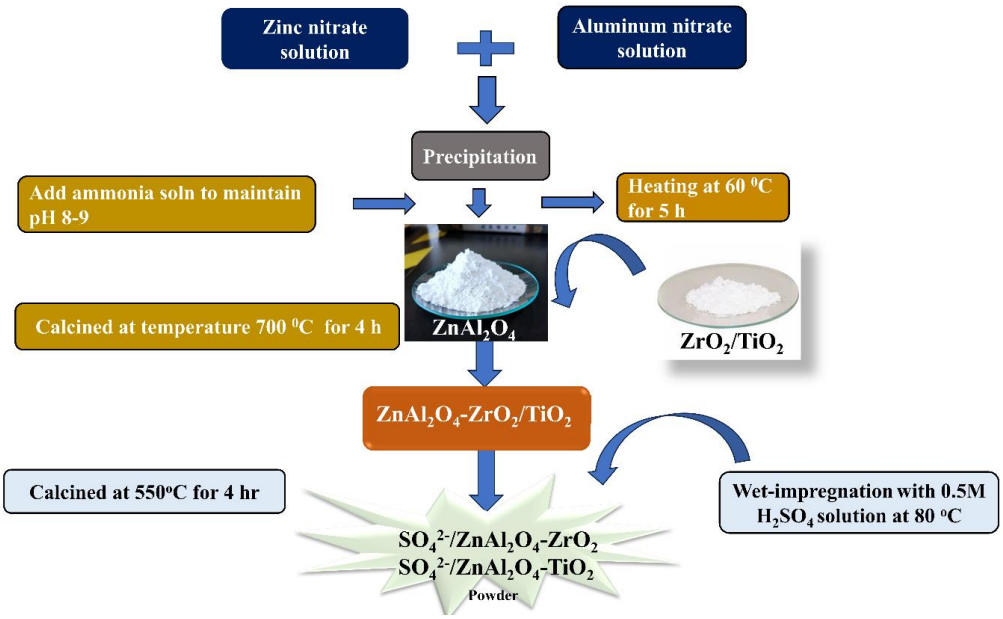

Scheme 6.1 Synthesis of SZA and SZZ catalyst

6.3 Characterization of synthesized catalyst

6.3.1. TGA analysis

The temperature disintegration versus mass loss of the uncalcined catalyst SZZ and SZT were studied by the thermogravimetric analysis in the presence of a nitrogen atmosphere. In Figure 6.1, three distinct phases of mass loss are evident as the temperature increases for the SZT catalyst. The initial phase of weight deduction, observed between 100-200 ^{o}C, can be owing to the dehydration of the surface water molecule adsorbed by the surface of the catalyst. The 2nd phase was observed around 200-550 ^{o}C, possibly due to the evaporation of the crystalline water molecules or any organic impurities. The 3rd stage of weight reduction occurred within the temperature range of 500 ^{o}C to 850 ^{o}C due to the decomposition of the surface sulfate group. So, the SZT catalyst showed 45 % mass weight loss above 550 ^{o}C. Similarly, the TGA curve of the SZZ catalyst is shown here. In the SZZ case, the initial phase of weight loss for the catalyst, occurring below 200 ^{o}C, could be assigned to removing physically bound water molecules. The 2nd weight loss observed between 200 ^{o}C and 550 ^{o}C is attributed to the release of structural water molecules. The 3rd stage of mass reduction was ascertained at a higher temperature range between 500-900 ^{o}C; it was observed that the gradual decomposition of the sulfate group from the catalyst surface [86,143]. Based on the TGA graph, the weight loss of the sample was estimated to be 36 %. The weight loss in the SZT catalyst above 550 ^{o}C was higher, which indicates the catalyst is highly unstable above that temperature. Whereas in the SZZ catalyst, the weight loss was estimated to be less (i.e., 36 %) than SZT catalyst. This happens because the SZZ catalyst surface was found to be more stable and decomposed in less extent above that temperature.

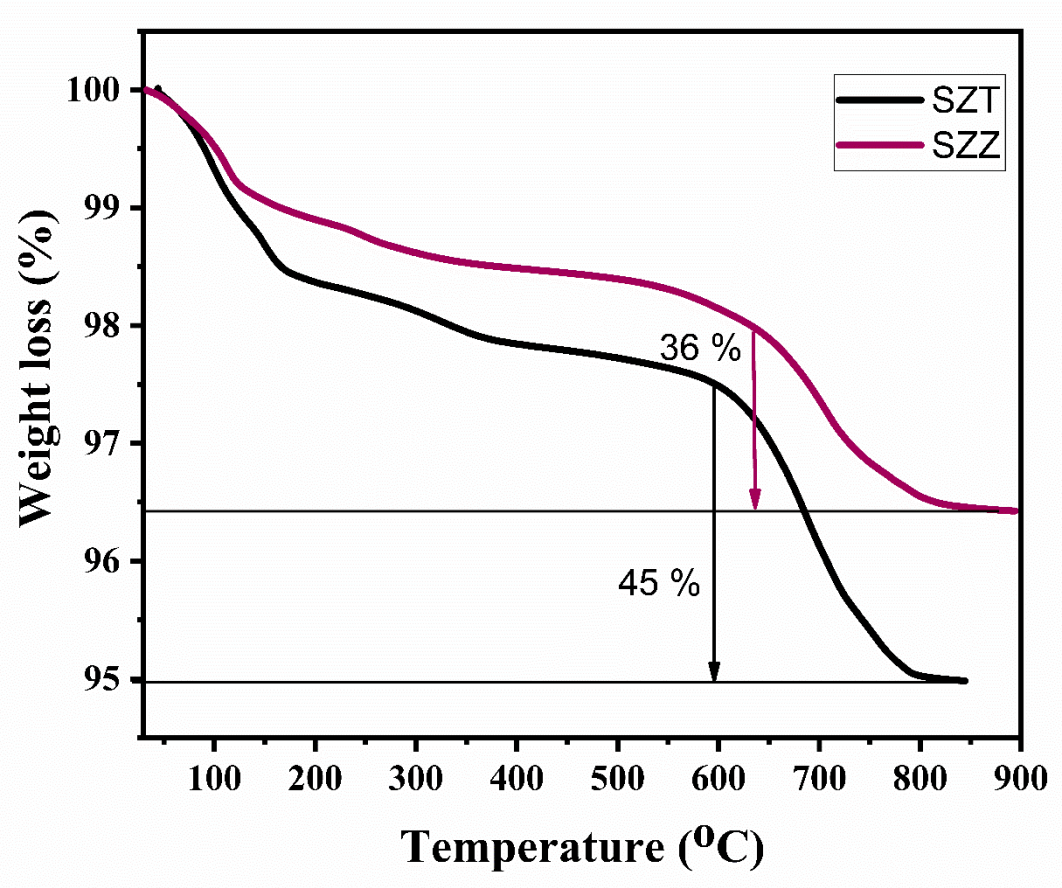

Figure 6.1 TGA graph of synthesized uncalcined SZZ and SZT catalyst

6.3.2. X-ray diffraction studies

The XRD technique studied the purity of the phase, crystalline structure, and orientation of the designed catalyst. Figure 6.2 (a) shows the XRD graph of the SZT catalyst. The characteristics diffraction peak appeared at 2 θ values equal to 31.2°, 36.8°, 44.9°, 49.0°, 55.5°, 59.4°, 65.2°, 74.2°, and 77.3° corresponding to the miller indices values (220), (311), (400), (331), (422), (511), (440), (620), and (533) respectively shows the orientation planes of cubic phase of $ZnAl_2O_4$ matched with the JCPDS card no. 05-0669. Another prominent peak appears at 25.3°, 37.8°, 47.9°, 53.7°, 54.9°, 62.7°, 68.8°, 70.3°, and 75.1° with Miller indices (101), (004), (200), (105), (211), (204), (220), and (215), respectively were all corresponds to the anatase phase of TiO_2 matched with the JCPDS no- 65-5714. Due to sulphonation, some minor $Al_2(SO_4)_3$ peaks are also observed at 2 θ

values 15.1°, 21.1°, and 25.2°, matched with the JCPDS no- 22-0021. This confirms the successful impregnation of the sulfate group on the SZT catalyst. Using Scherrer's equation, the crystalline size of the SZT catalyst was determined to be 23.03 nm.

$$D = \frac{0.9\,\lambda}{\beta cos\theta} \qquad (6.1)$$

Where D denotes the average crystallite size, β corresponds to the line broadening at FWHM, θ is the diffraction Bragg angle, and λ refers to the wavelength of the X-ray. Similarly, in Figure 6.2 (b), the XRD pattern of the SZZ catalyst is depicted. The predominant diffraction peaks of tetragonal ZrO_2 were observed at 2 θ of 30.1°, 35.2°, 50.3°, 60.2°, 62.7°, and 74.5° consisting of the hkl planes of (101), (110), (112), (211), (202), and (220) respectively matched with the JCPDS card no- 88-1007. Some minor peaks of $Al_2(SO_4)_3$ also appeared on the surface of the SZZ catalyst at 15.0°, 20.8°, and 25.1°, corresponding to the miller indices (012), (104), and (113) (JCPDS no-22-0021). The crystalline size of the SZZ catalyst was observed to be 46.29 nm using the above Scherrer's equation [144]**.** The diffraction peaks of SZZ catalysts are sharper and more intense than SZT catalysts, indicating that SZZ catalysts are more crystalline. The higher crystallinity might cause a higher glycerol conversion to solketal.

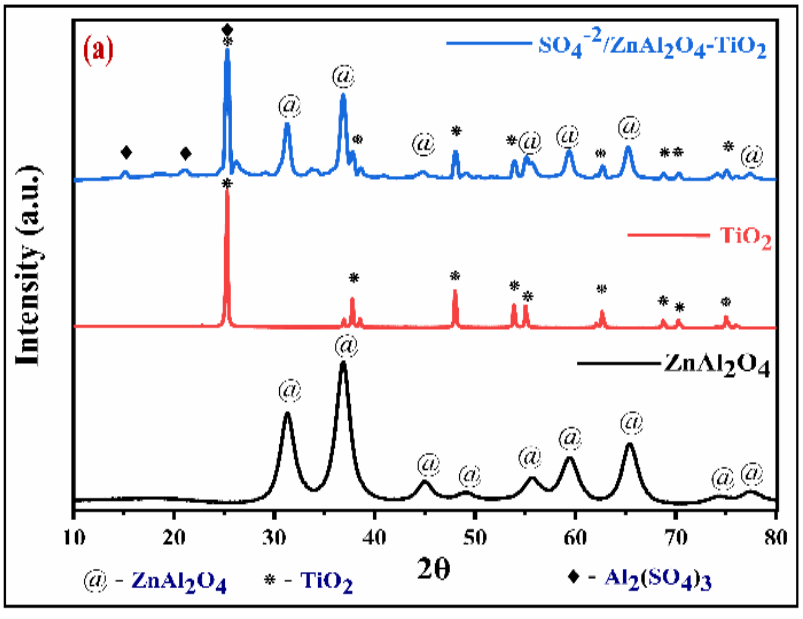

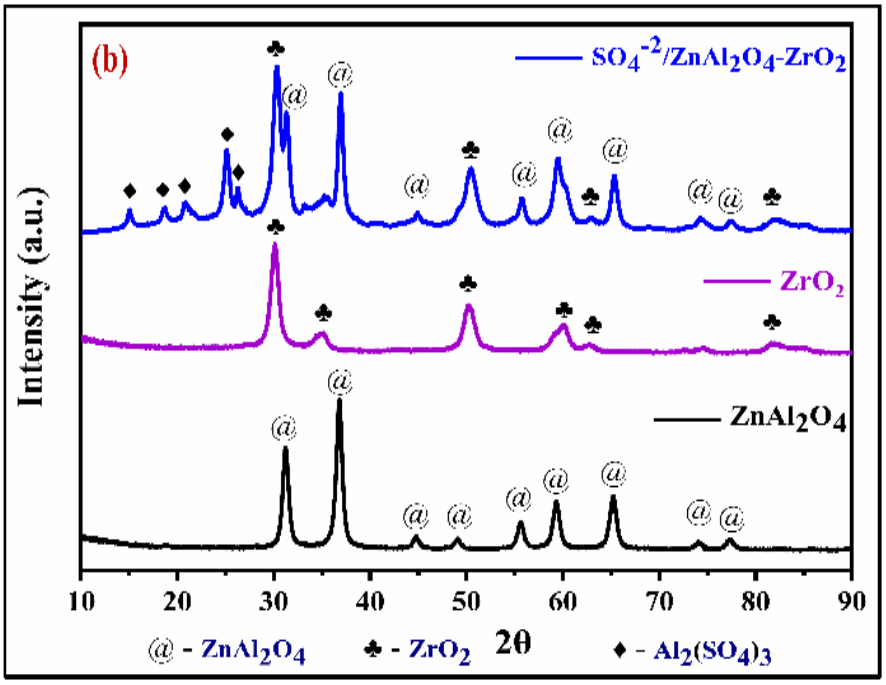

Figure 6.2 XRD patterns of (a) SZT, (b) SZZ catalyst

6.3.3. FTIR spectra

The existence of the functional group on the catalyst surface plays a crucial role in the glycerol conversion, which was studied by the FTIR analysis. Figure 6.3 shows the FTIR pattern of the SZT and SZZ catalysts. The characteristic peaks observed between 500 cm^{-1} and 670 cm^{-1} indicate metal-oxygen and metal-oxygen-metal bonding. The low-frequency absorption band appeared at ~ 490, 535, and 660 cm^{-1}, corroborating the Zn-O-Al, Al-O, and Zn-O bond in SZT and SZZ, respectively. The stretching vibrations band of Zr-O was detected at 600 cm^{-1} and 725 cm^{-1} in SZ and SZZ catalysts [145]**.** Similarly, the vibration mode of the Ti-O-Ti bond appeared in the range of 400-800 cm^{-1} in ST [146]**.** The peaks originating at 1006 and 1102 cm^{-1} were depicted as the symmetric and asymmetric stretching of S-O bonds, respectively. Other peaks around 1250 cm^{-1} could be evident attributed to the stretching vibration of S=O bonds, indicating the formation of a bidentate chelating structure between sulfate and metal ions. In addition, 1630 cm^{-1} and 3460 cm^{-1} peaks assigned the -OH bending and stretching vibration of the adsorbed water

molecule on the catalyst's surface, respectively [147].

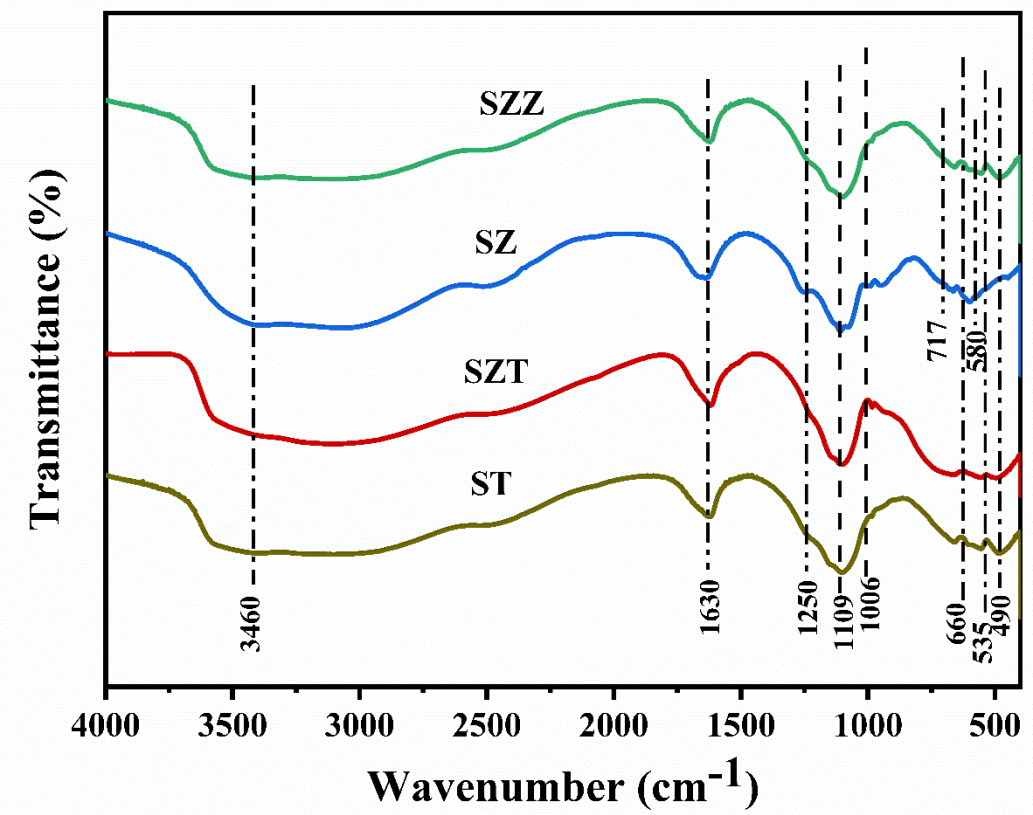

Figure 6.3 FTIR spectra of ST, SZT, SZ, and SZZ catalyst

6.3.4. SEM-EDX analysis

The structural characteristics and surface topology of the SZZ and SZT catalysts were viewed using SEM (Scanning electron microscope) techniques. Figure 6.4 (a) depicts the morphology of the SZZ catalyst, showing a homogeneous distribution of both grains in variable size. The bulk grain particles of ZrO_2 are finely dispersed across the spherical surface of $ZnAl_2O_4$. This outcome clearly showed that both $ZnAl_2O_4$ and ZrO_2 were successfully composited on the $SO_4^{2-}/ZnAl_2O_4$-ZrO_2. ZrO_2 helps prevent the agglomeration of $ZnAl_2O_4$ particles and facilitates the dispersion on SZZ solid acid catalyst, improving the surface area that is highly suitable for acetalization reaction. The atomic ratio of the catalyst was cross-verified by the EDX (Energy-dispersive X-ray) spectroscopy. The EDX histogram of SZZ reveals the existence of elements like Zn, O,

Zr, Al, and S on the catalyst surface, as indicated by their atomic and weight percentage [148,149]. On the other hand, Figure 6.4 (b) depicts the surface morphology of SZT. It was found that the plate-like morphology of TiO_2 was not homogenously mixed with spherical particles of $ZnAl_2O_4$, revealing that particles are not uniformly scattered on the SZT surface. As a result, the particle size of SZT is larger, which decreases the surface area. Consequently, SZT has lower catalytic activity than SZZ towards glycerol acetalization. The EDX histogram confirms the synthesis of SZT on the basis of their atomic percentage present on designed catalyst surfaces like Zn, Al, Ti, O, and S [150].

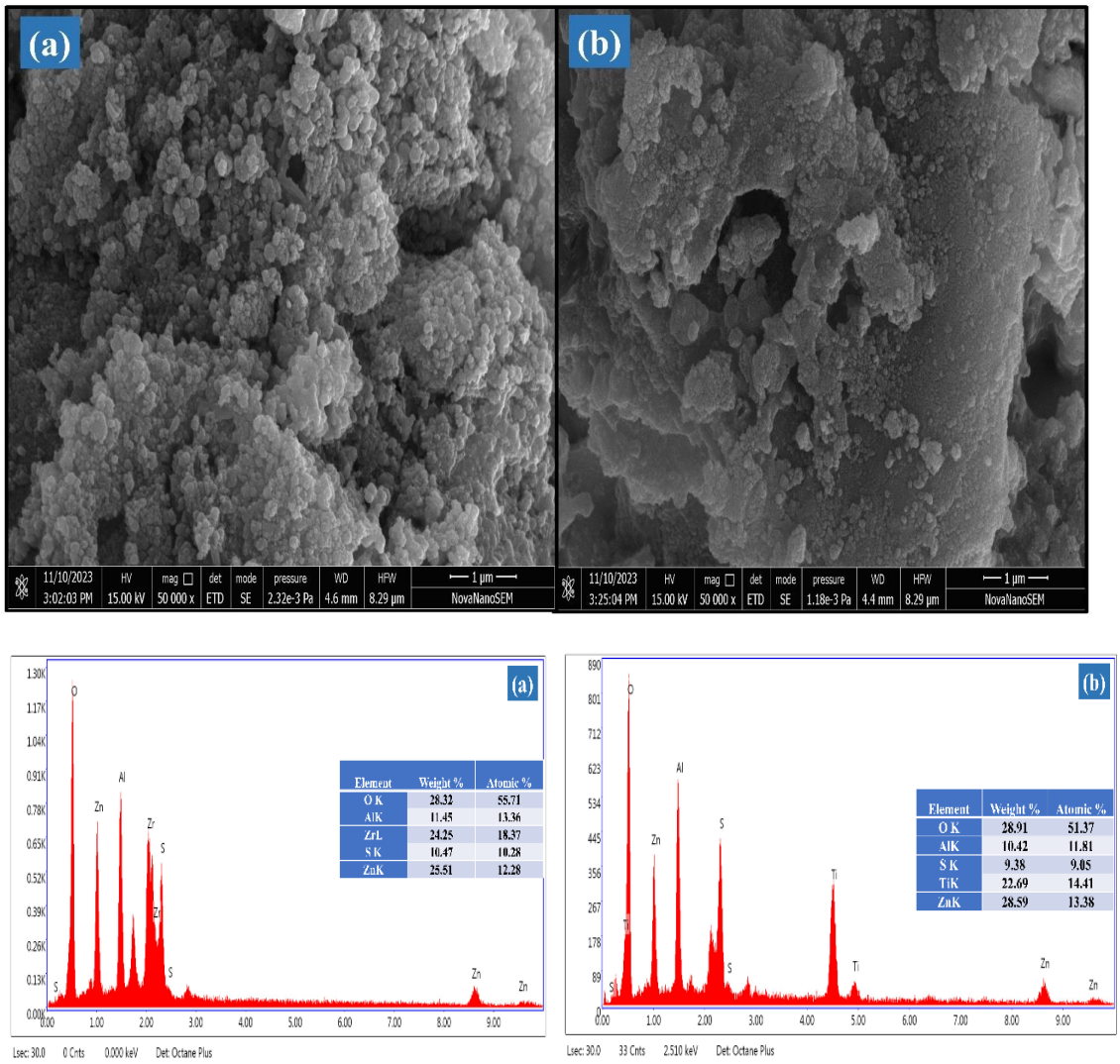

Figure 6.4. SEM-EDX image of (a) SZZ, (b) SZT catalyst

6.3.5. BET surface area analysis

The specific surface area of the synthesized catalyst plays a crucial role in the glycerol acetalization reaction. Acidity and surface area both affect the solketal synthesis. Nonetheless, acidity is a more prominent factor than surface area analysis. The surface area of both catalysts SZT and SZZ were tentatively quantified by BET nitrogen adsorption-desorption isotherm, and the obtained plot is illustrated in Figure 6.5 (a) and (b), respectively. Similarly, pore diameter and pore volume were also elucidated through the BJH (Barrett-Joyner-Halenda) method. The surface area, along with pore diameter and pore volume of SZT and SZZ catalyst, is enlisted in Table 2. It was found that the calculated specific surface area of the SZT catalyst is 2.5 m^2/g, and that of SZZ is 5.5 m^2/g. This indicates that SZZ has a higher surface area than SZT. Likewise, the pore diameter and pore size of SZZ were found to be larger than those of SZT. Both catalysts follow a type IV isotherm with an H1-type hysteresis loop. This signifies that materials belong to mesoporous in nature (2-50 nm). The higher specific surface area of the SZZ catalyst facilitates the acetalization reaction of glycerol. It is recognized that the glycerol acetalization reaction with a catalyst is a surface adsorption phenomenon. As a result, the SZZ catalyst with a higher surface area boosted the higher glycerol conversion than SZT catalyst [151].

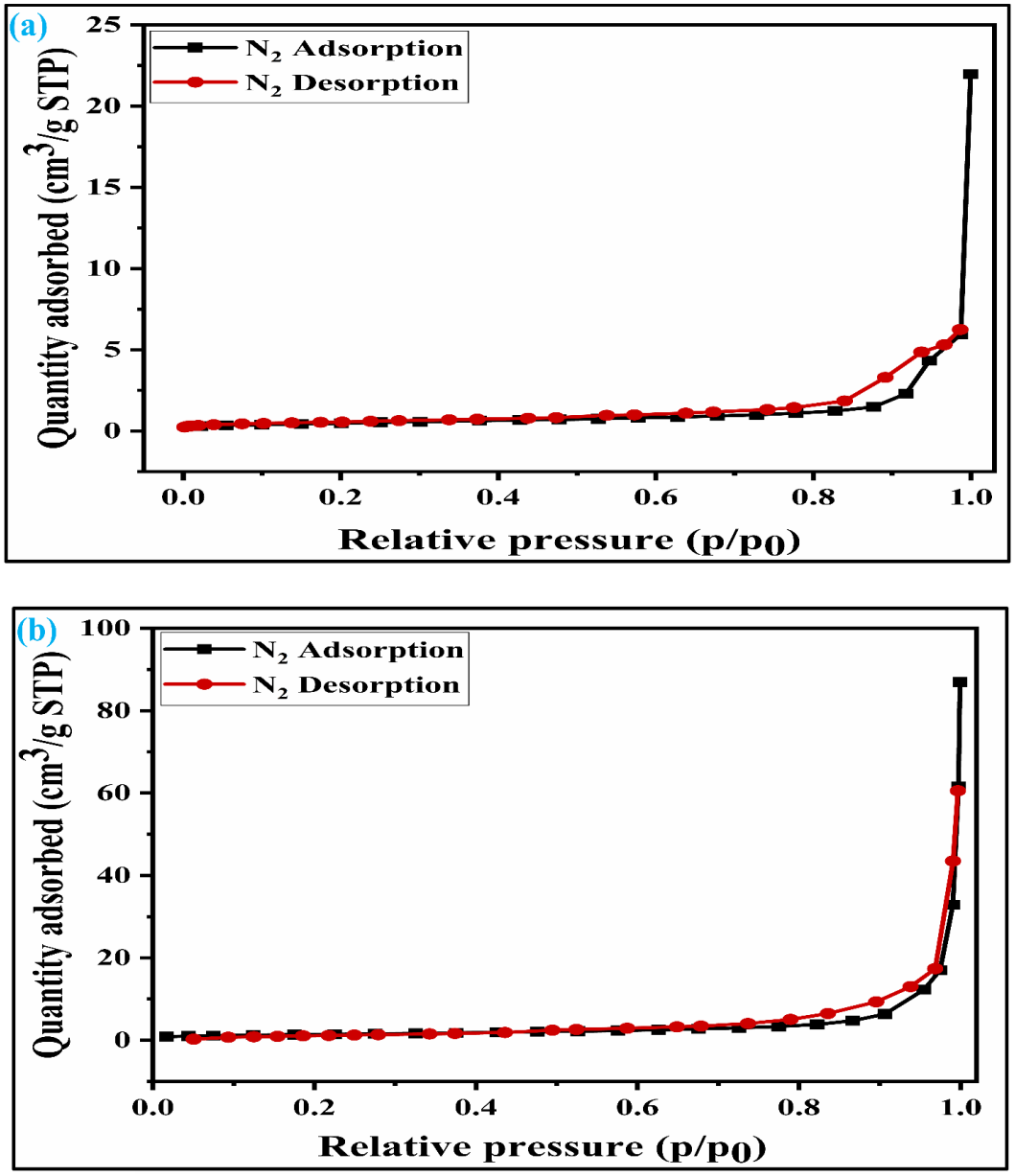

Figure 6.5 Nitrogen adsorption and desorption isotherm of (a) SZT catalyst and (b) SZZ catalyst

6.3.6. XPS analysis

The surface analysis of the SZZ and SZT catalysts was investigated by X-ray photoelectron spectroscopy (XPS). The XPS technique was employed to determine the material's oxidation state and chemical composition. Figure 6.6 (a) displays the XPS spectra of the SZZ catalyst that indicate the presence of Zn, Al, O, Zr, and S on the catalyst surface. The distinctive peaks that appeared at 183.5 eV and 185.9 eV, corresponding to

the Zr $3d_{5/2}$ and Zr $3d_{3/2}$, respectively, corroborated that Zr is present in the (IV) oxidation state. The O1s spectrum reveals three deconvoluted peaks corresponding to different binding energy states. The first peak appeared at 530.1 eV, which can be associated with lattice oxygen involved in metal-oxygen bonding, while the peak at 531.5 eV is assigned to the bridged oxygen of the -OH group. Moreover, the peaks observed at 532.5 eV correspond to the sulfate oxygen group. In the Zn 2p spectrum, the characteristics peak appeared at 1021.5 eV, which signifies Zn $2p_{3/2}$, while the peak at 1044.8 eV corresponds to Zn $2p_{1/2}$, which shows the existence of Zn in the +2-oxidation state, which was close to standard data. The peak appeared at 75.3 eV, which corresponds to the +3 oxidation state of Al. S 2p spectra exhibit two distinct peaks, one appearing at 169.4 eV and the other at 170.2 eV. These peaks are attributed to the binding energies of S $2p_{3/2}$ and S $2p_{1/2}$, respectively, which were associated with the +6 oxidation state of the sulfur [152,153]. The presence of Zn, Al, Ti, O, and S in the SZT catalyst was depicted in Figure 6.6. (b). The presence of aluminum in the +3 oxidation state is indicated by the peak observed at 75.2 eV in the spectra. The deconvoluted peak that appeared at binding energy 1045.8 eV resembles Zn $2p_{1/2}$, and 1022.7 eV corresponds to Zn $2p_{3/2}$, showing the +2-oxidation state of Zn. In the Ti spectrum, Ti 2p peaks are observed at binding energies 459.1 eV and 464.5 eV associated with the Ti $2p_{3/2}$ and Ti $2p_{1/2,}$ respectively. These peaks exhibit a doublet splitting of 5.7 eV caused by the spin-orbit coupling of Ti 2p, which indicating the +4-oxidation state of titanium. In the O 1s spectrum, three characteristic peaks were observed: one at 530.4 eV corroborated to the lattice metal-oxygen bonding, another at 531.4 eV associated with the bridged oxygen of the hydroxyl group, and a third peak at 532.3 eV linked to the sulfate oxygen group. In S 2p spectra, the binding energies of S $2p_{3/2}$ and S $2p_{1/2}$ were obtained at 169.4 eV and 170.2 eV, assigned to the +6 oxidation state of the bidentate sulfur group [154]. The comparison of the area ratios [O ads] / [O

lat] allows for the evaluation of the relative quantities of two distinct oxygen species. A greater area ratio suggests a higher concentration of oxygen vacancies, whereas a smaller area ratio suggests fewer oxygen vacancies [155]. In this context, [O ads] / [O lat] area ratio for SZZ catalyst is higher compared to SZT catalyst. Consequently, SZZ exhibits a relatively higher concentration of surface and unoccupied oxygen compared to SZT.

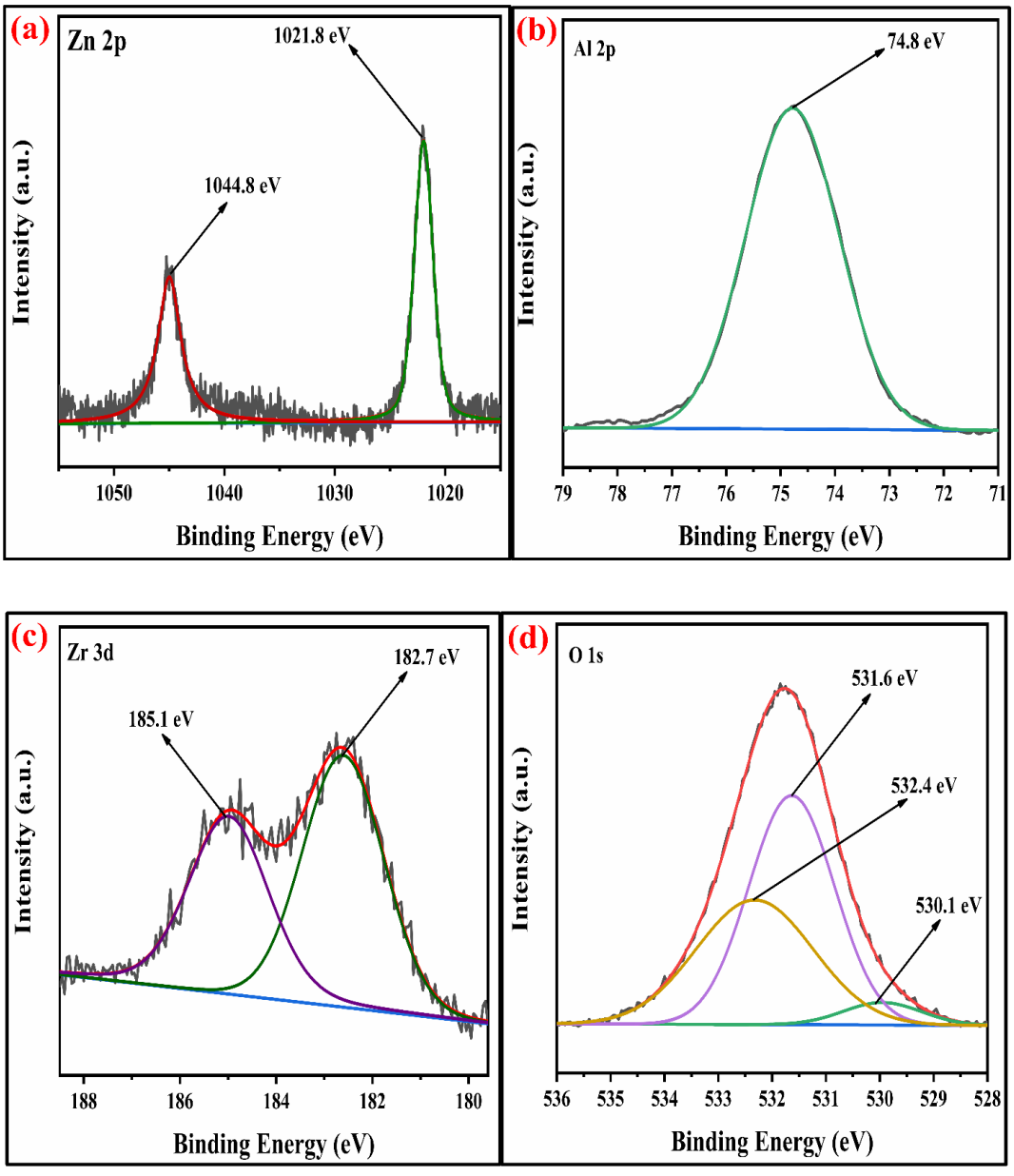

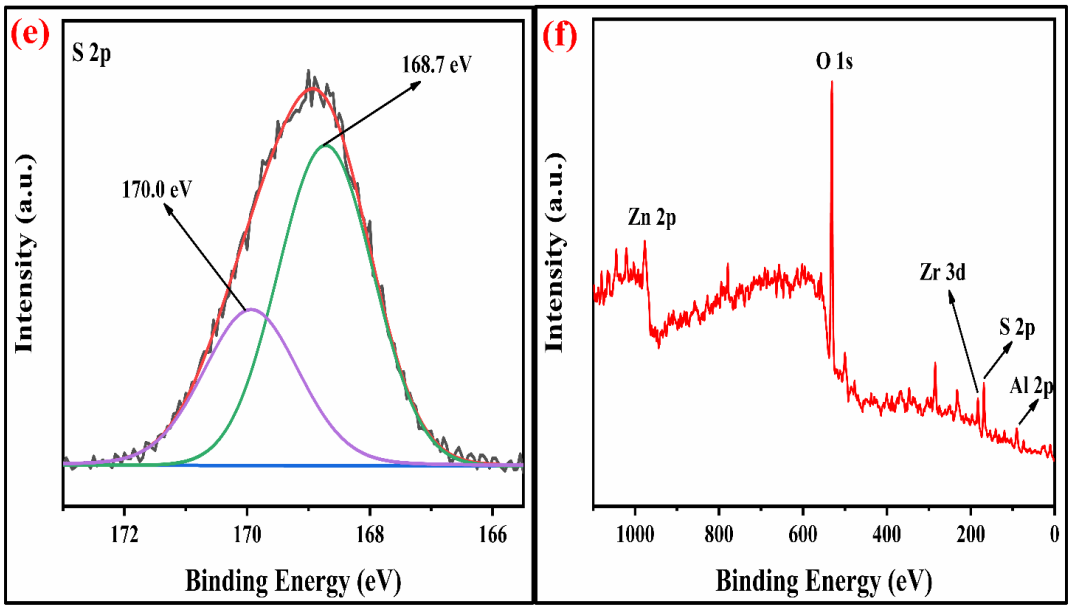

Figure 6.6 (a). XPS spectra of (a) Zn 2p, (b) Al 2p, (c) Zr 3d, (d) O 1s, (e) S 2p, and (f) survey peak of SZZ catalyst and

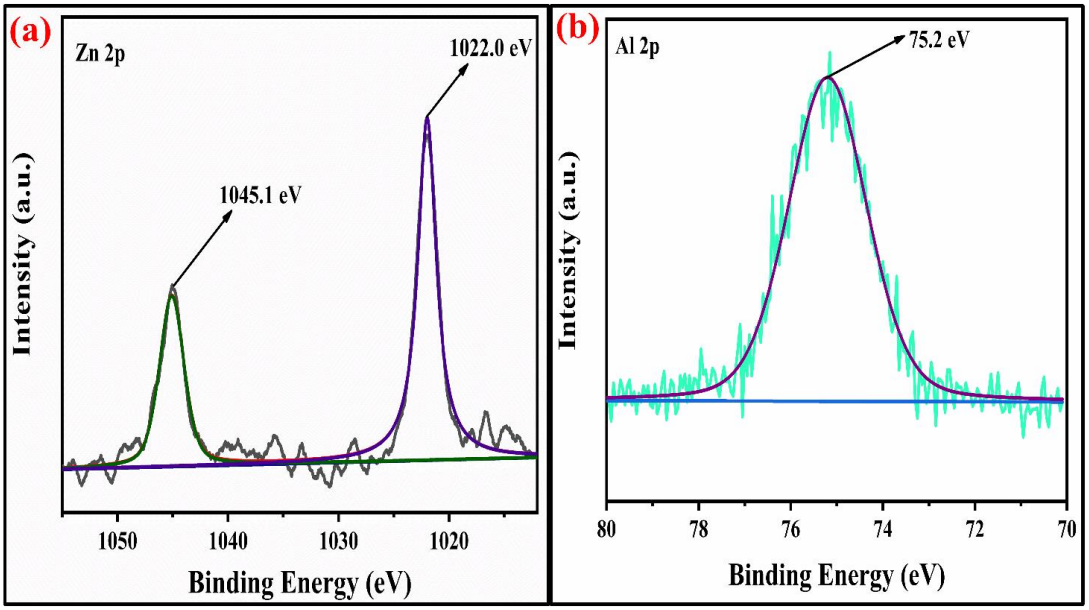

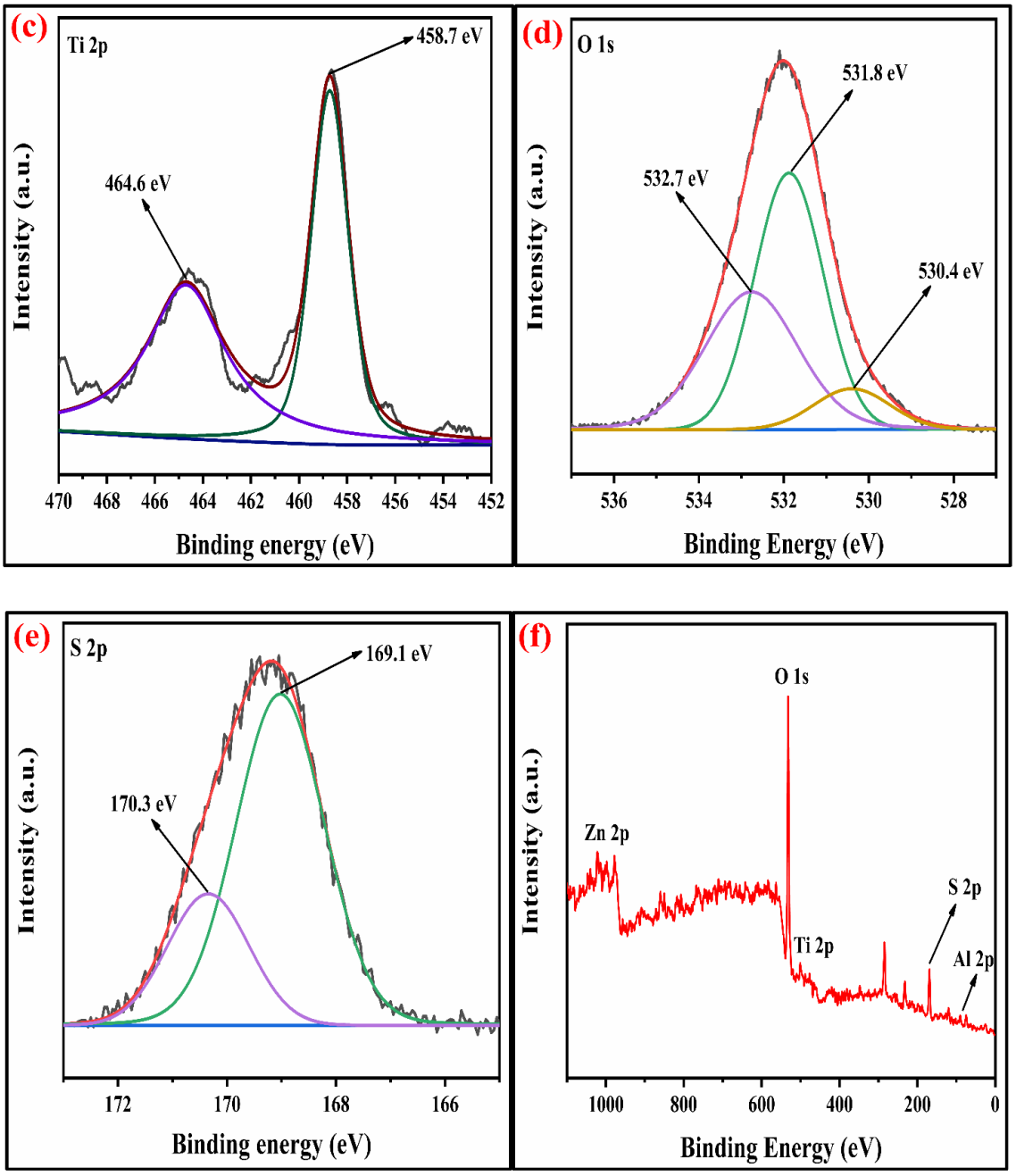

Figure 6.6 (b). XPS spectra of (a) Zn 2p, (b) Al 2p, (c) Ti 2p, (d) O 1s, (e) S 2p, and (f) survey peak of SZT catalyst

6.3.7. Acidity of the synthesized catalyst

Synthesis catalyst's acidity and acidic strength are crucial in glycerol acetalization reaction. As a result, the catalyst's active site protonates the carbonyl carbon, increases the electrophilicity, and further proceeds the reaction. Here, we

performed the N-butylamine titration process to estimate the overall acidity of the catalyst quantitatively, and the obtained results are illustrated in Table 6.1. The obtained result showed that SZZ had more acidic sites than SZT. Given that the acetalization reaction of glycerol with acetone relies on an acidic catalyst, the higher acidity of SZZ contributed to improved glycerol conversion [13].

Table. 6.1 Surface properties and acidic sites of the catalyst

Catalyst	Surface area(m^2/g)[a]	Pore volume (cm^3/g)[b]	Average pore diameter (nm)[c]	Acidic sites (mmol/g)[d]
SZZ	5.3	0.05	39.4	2.87
SZT	3.9	0.01	31.8	2.35

[a] The specific surface area was determined using BET method.

[b] Pore volume was calculated by the amount of adsorbed nitrogen (p/p_0=0.990).

[c] Average pore diameter was deliberated by using BJH method.

[d] Acidity was determined by N-butylamine titration.

6.4 Catalytic evaluation for solketal synthesis

The acetalization reaction between glycerol and acetone was executed in a 250 ml round bottom flask associated with the reflux condenser and a mechanical stirrer (Tarson digital spinout). The reactor setup was immersed in a silica oil bath for continuous heating. Initially, 2.5 mmol and 25 mmol of glycerol and acetone were introduced along with catalyst loading of 3 wt.% of catalyst loading (relative to glycerol) at the optimum reaction temperature of 70 ^oC for 120 min. Following the reaction completion, the resulting mixture was cooled and separated from the solid catalyst using centrifugation. The quantitative validation of the synthesized solketal was studied through gas

chromatography-mass spectrometry (GCMS) using Agilent Technologies 7890B GC coupled with an MS of 19091P-MS4 system associated with an HP-5 capillary column with flame ionization detector (FID). Initially, the oven temperature was set to 80 ^{o}C, then ramped up at a rate of 20 ^{o}C/min to 220 ^{o}C. The injector and detector temperatures were optimized and maintained at 250 ^{o}C and 300 ^{o}C, respectively. 1,4-dioxane served as an internal standard in solketal synthesis for GC analysis. The percentage conversion of glycerol, selectivity, and yield of the solketal was determined by providing the following equation. Additionally, verification of solketal synthesis was carried out using ^{1}H, and ^{13}C NMR spectroscopy as well as FTIR spectroscopy [54,156].

The turnover frequency for the $SO_4^{2-}/ZnAl_2O_4$-ZrO_2 and $SO_4^{2-}/ZnAl_2O_4$-TiO_2 catalysts were observed to be 0.1 mol $g^{-1}h^{-1}$ and 0.17 mol $g^{-1}h^{-1,}$ respectively**.** The synthesized catalysts were applied for solketal synthesis and obtained conversion and selectivity, as shown in Table 6.2.

Table 6.2. Screening of catalyst for the synthesis of solketal with time

Catalyst	Conversion (%)	Solketal selectivity (%)	TOF (mol g^{-1} h^{-1})
SZZ	99	99	0.19
SZT	83	96	0.17

6.4.1. Characterization of synthesized product

6.4.1.1. ^{1}H and ^{13}C NMR analysis

The NMR spectroscopy characterized the acetalization product of glycerol. The chemical identity of the synthesized product was validated through NMR analysis, and the obtained characteristic peaks were compared to the corresponding peak with the reactant and product. Figure 6.7 (a) displays the ^{1}H and Figure 6.7 (b) ^{13}C NMR spectra of the solketal.

In ^{1}H NMR spectra, two singlet characteristic peaks of six methyl hydrogen were observed at chemical shift values of 1.26 and 1.30 ppm, while a broad singlet peak at 2.0 ppm is attributed to the hydroxyl (-OH) moiety. The multiple peaks of the chemical shift value of 3.36 to 4.80 ppm represent the -CH and -CH_2 groups' integration of the five-membered solketal ring**.** In ^{13}C NMR spectra the characteristics peak was noticed at 25.77 and 27.11 ppm, which were attributed to the -CH_3 carbon within the cyclic product. The chemical shift value obtained at 76.52 and 76.78 ppm assigned for the -CH_2-CH-CH_2- carbon, while two additional peaks were noted at 66.58 ppm and 62.67 ppm assigned to the two -CH_2 carbon of the cyclic ring. The highly deshielded peak that emerged at 108.56 ppm indicates the ketal carbon that corroborates the formation of solketal as a product. Additionally, extra multiplet peaks that appeared at 39.65 ppm are associated with the DMSO-d6 solvent**.**[157] The ^{1}H and ^{13}C NMR of synthesized solketal were acquired using a BRUKER Bio Spin 500, Advance III HD 500 MHz spectrometer.

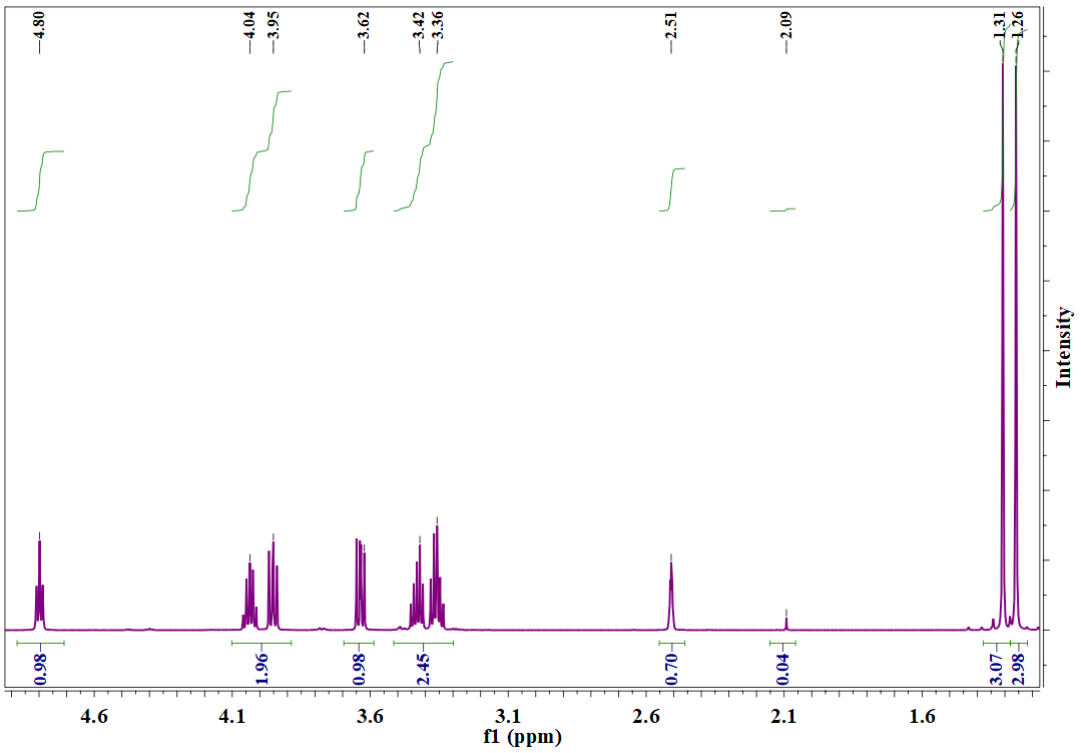

Figure 6.7 (a) ^{1}H NMR spectra and

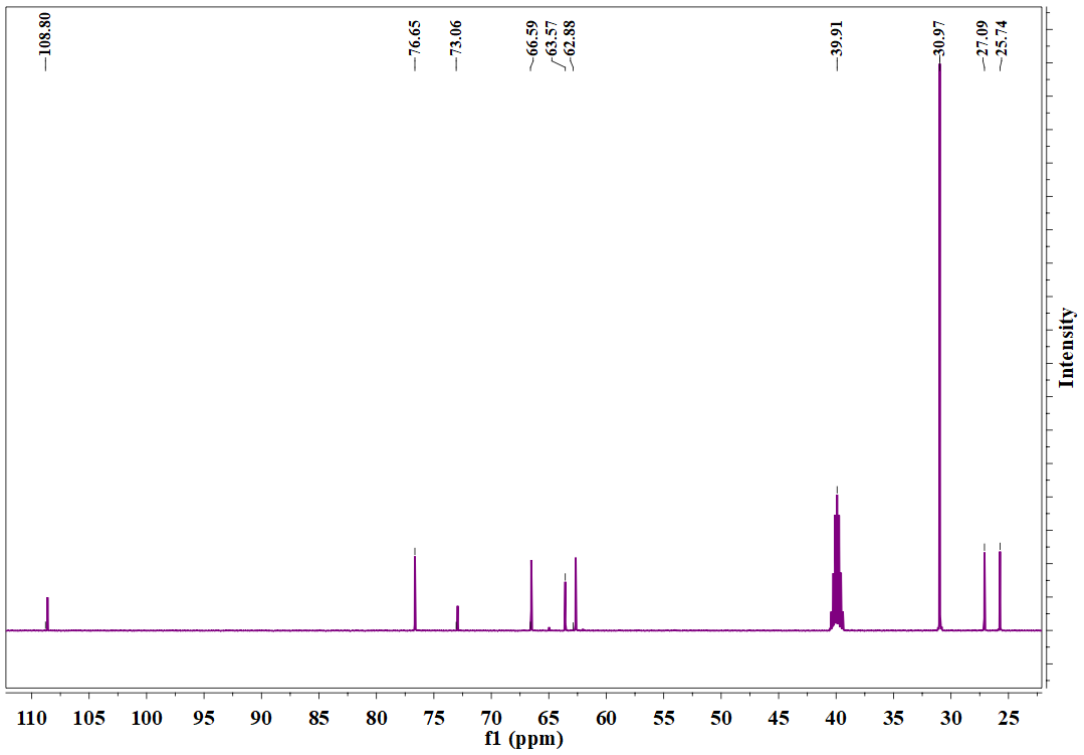

(b) ^{13}C NMR spectra of solketal

6.4.1.2. GCMS studies

Gas chromatograph-mass spectroscopy is a robust analytical method employed to identify the composition of products within an analytical mixture. The qualitative and quantitative investigation of the synthesis product was performed using the GC-MS studies and illustrated in Figure 6.8. The retention peak confirmed the production of five-membered solketal, which was found at 3.98 min. while others demonstrated the formation of six-membered acetal at 4.31 min. A tiny amount of unreacted glycerol was found at the peak at 4.78 min.

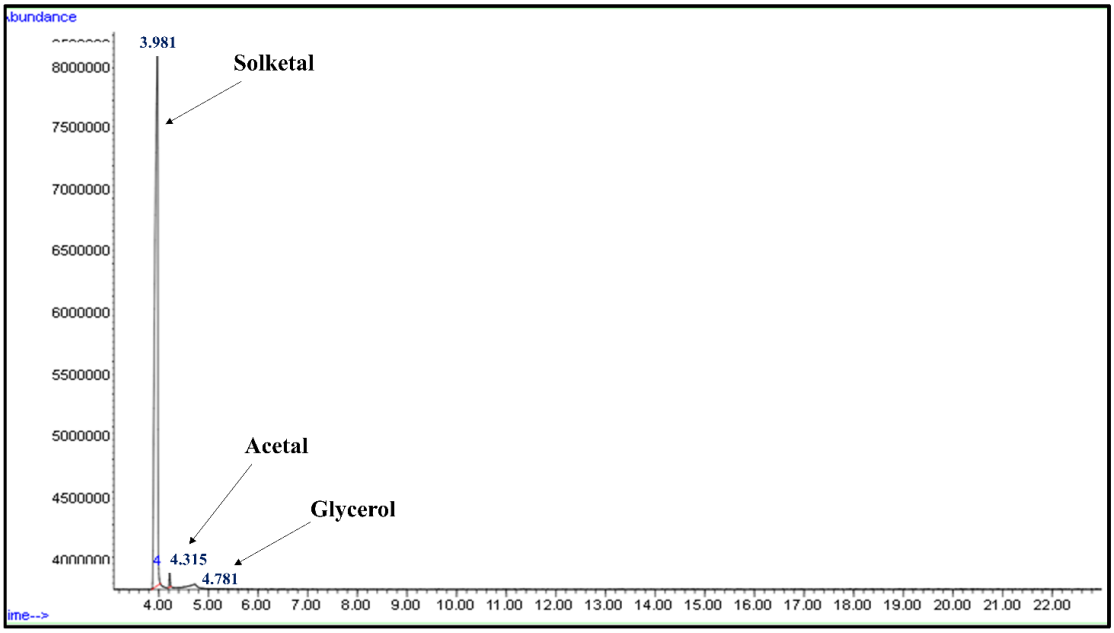

Figure 6.8 GCMS spectra of the synthesized product

6.4.1.3. FTIR analysis

Solketal synthesis was also verified by FTIR spectroscopy. The FTIR spectra of both glycerol and synthesized solketal are shown in Figure 6.9. Figure 6.9 (a) shows the FTIR spectrum of glycerol. The hydroxyl group's O-H stretching is allocated to a broad peak at 3408 cm^{-1}, while the glycerol absorption peak, which falls between 2885 and 2942 cm^{-1}, signifies the C-H stretching. The peak regarding C-O-H bending vibration was at 1419 cm^{-1}. The peaks with low intensity at 1111 cm^{-1} were assigned to the stretching band of C-O in 1^{o} alcohol, whereas the peak at 913 cm^{-1} owed to the bending vibration of the O-H group within the glycerol moiety.

The synthesized solketal's FTIR spectrum is depicted in Figure 6.9 (b). The noticeable peak was observed at ~ 3427 cm^{-1}, owing to the hydroxyl bonds (-OH) of solketal molecules. The intensity of this band is comparatively lower than that of glycerol, indicating that glycerol is converted to solketal. Within the range of wave numbers between 2881 and 2987 cm^{-1}, regarded as stretching of the C-H methyl bonds. Another peak was observed at 1376 cm^{-1}, which signifies the "umbrella" trend associated with the

ketone's methyl group. Band 1212 cm^{-1} represents the dioxolane -C-O bond. The asymmetric bands found at 1155 and 1116 cm^{-1} are accredited to the -C-O-C-O-C- bonds, while the peaks at 906 and 788 cm^{-1} are allocated to the symmetric vibration of the same bond within a solketal ring. Additionally, the band at 1042 cm^{-1} is attributed to the -C-C-OH bond in the 4th position of the alcoholic group [54]. Several characteristic bands, such as 1045, 1156, 1216, and 1380 cm^{-1}, were not found in glycerol FTIR spectra, which indicates the synthesis of solketal from glycerol.

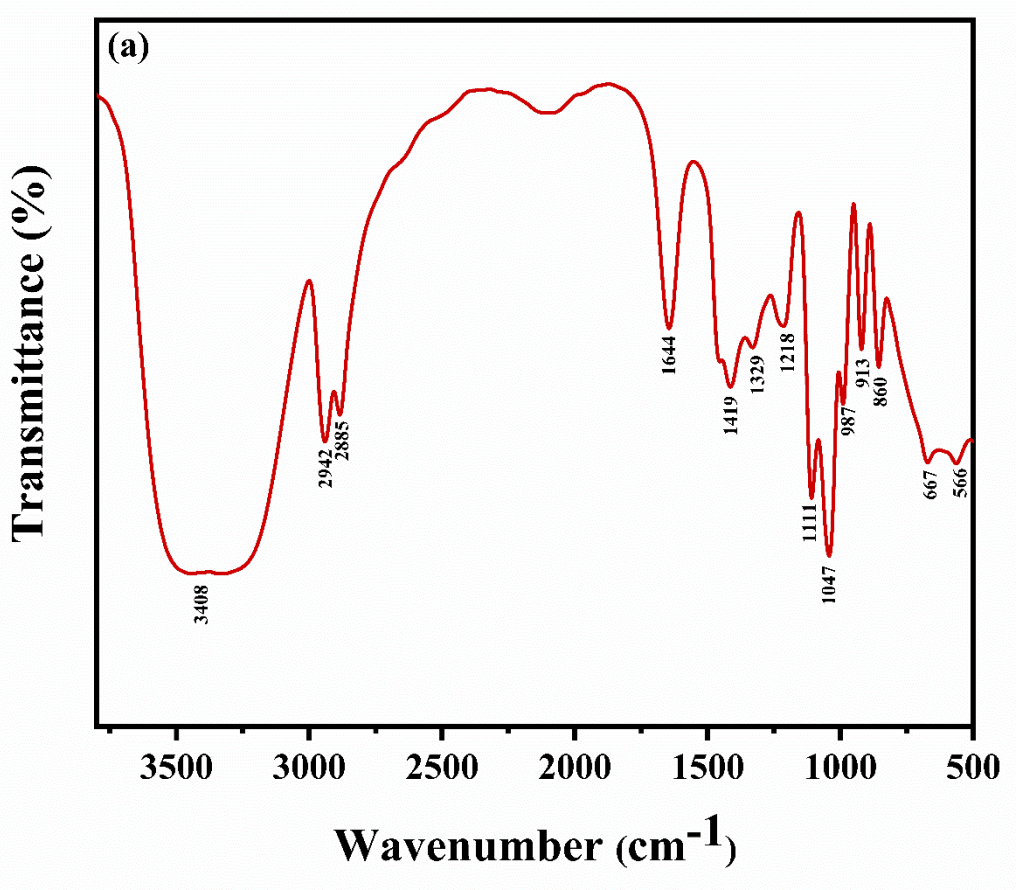

Figure 6.9. (a) FT-IR spectra of glycerol and

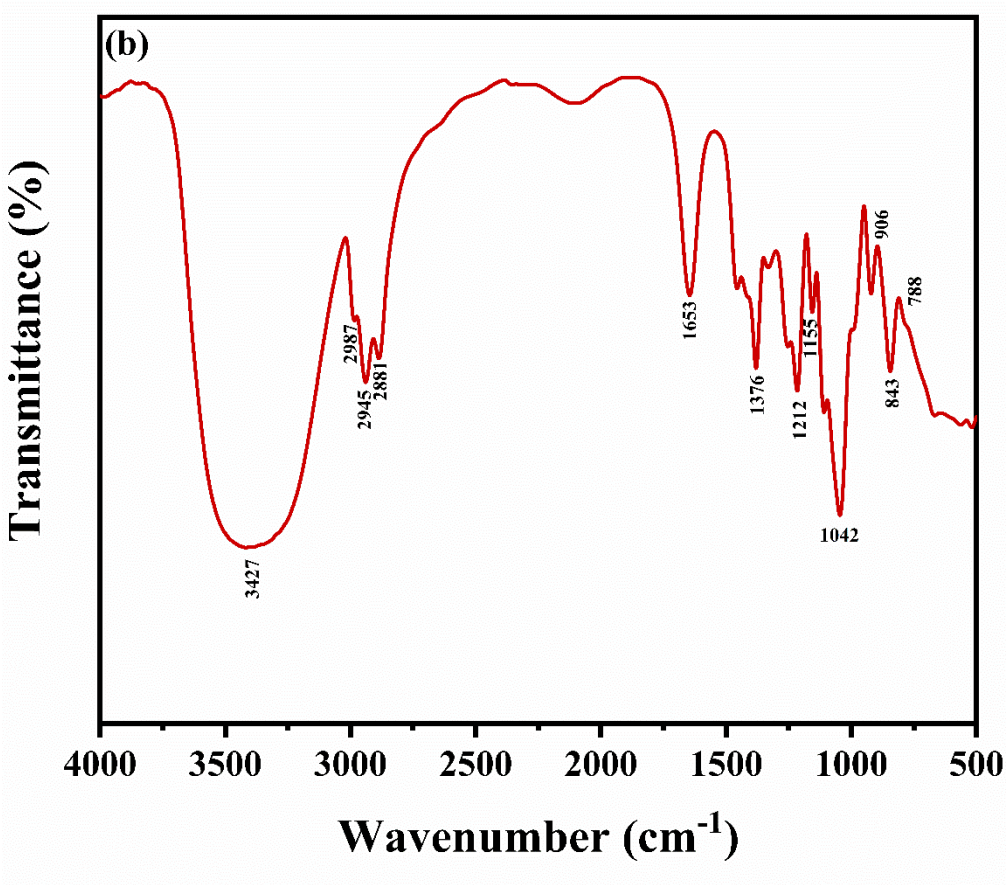

Figure 6.9. (b) FT-IR spectra of synthesized product

6.5 Proposed reaction pathway for solketal synthesis

The mechanist pathway of acetalization reaction using $SO_4^{2-}/ZnAl_2O_4$-ZrO_2 acid catalyst is designed by drawing upon previously documented literature. The Langmuir-Hinshelwood (L-H) model was selected as the most effective in describing the mechanism of this reaction, which goes through several phases illustrated in Figure 6.10. At first, reactant molecules (glycerol and acetone) are diffused on the catalyst surface, where they are adsorbed into the pores. In the first phase, acetone's carbonyl carbon undergoes protonation by the SZZ catalyst's acidic sites, enhancing the electrophilicity of carbonyl carbon. Subsequently, the second phase involves glycerol's hydroxyl group, which acts as a nucleophile, which initiates an attack on the most electrophilic carbon center of carbonyl group. The third phase is attended by deprotonation, leading to a highly unstable

hemiacetal intermediate. This intermediate undergoes cyclization by eliminating water molecules and engaging in an SN_2 nucleophilic substitution via two pathways. A five-membered solketal is created if the intermediate is attacked by the glycerol's secondary -OH group. Conversely, cyclization occurs by forming six-membered acetals by attacking the primary- OH group. Notably, kinetic parameters favor the five-membered cyclic solketal over the six-membered acetal, making the solketal a major product in this reaction pathway.[140]

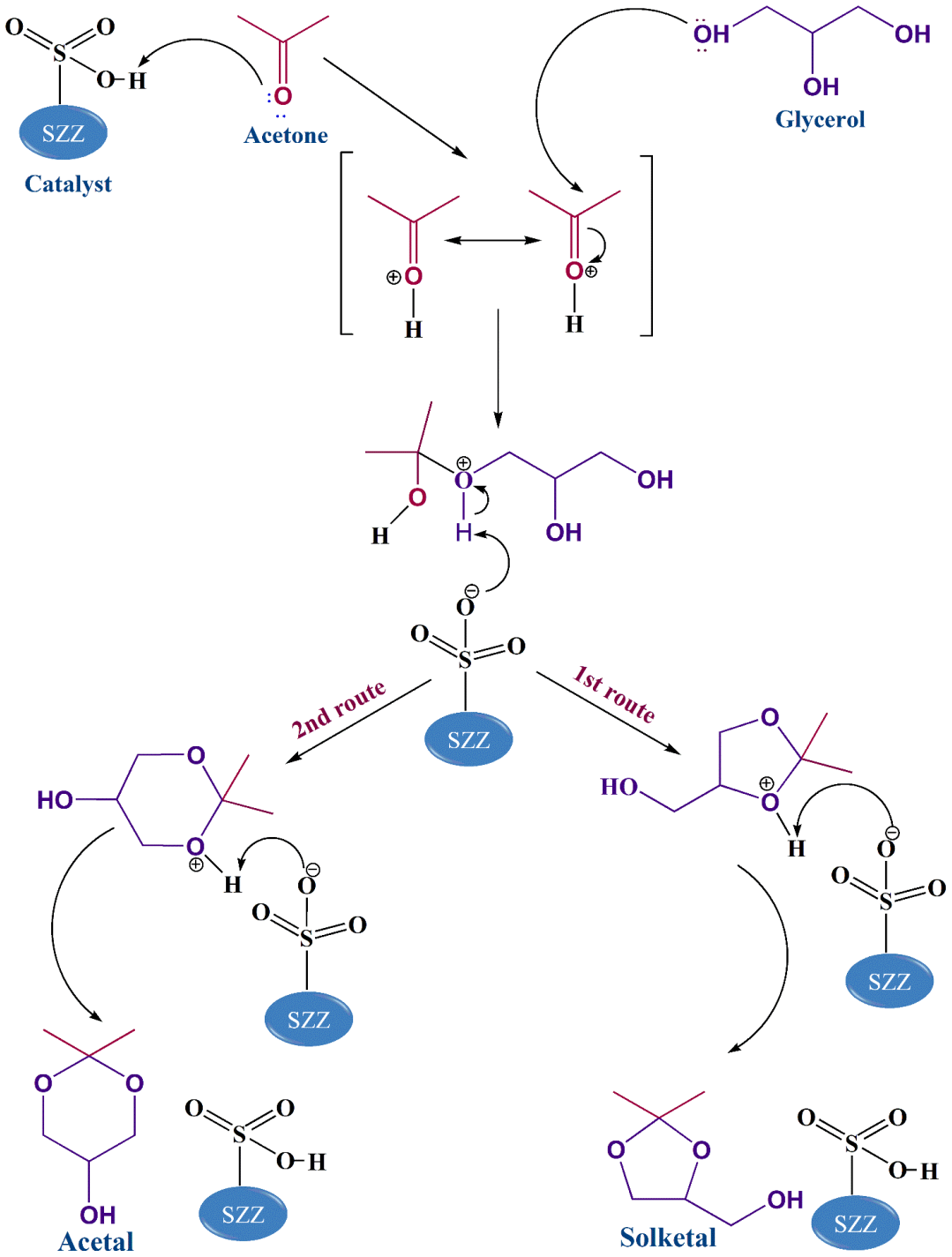

Figure 6.10 Mechanistic demonstration of the acetalization of glycerol using catalyst

6.6 Studies of optimization reaction parameters on solketal yield

6.6.1. Optimization of temperature in solketal synthesis

The reaction temperature, being one of the key factors that influence glycerol conversion,

was also optimized by fluctuating temperature from 40 ^{o}C to 80 ^{o}C. In contrast, all other parameters remained constant, as revealed in Figure 6.11 (a). The optimum temperature for the highest conversion of glycerol is 70 ^{o}C. This temperature provides a sufficient amount of kinetic energy to the reactants, which accelerates the glycerol acetalization reaction. It was found that both the glycerol conversion and percentage yield of the solketal increased as the temperature rose from 40 ^{o}C to 70 ^{o}C. This temperature increase facilitates the collision between the reactant molecules, consequently promoting conversion. However, above 70 ^{o}C, the conversion and yield percentages began to decrease. This decline can be ascribed to the evaporation of the acetone molecule from the reaction matrix. Consequently, an incomplete acetalization reaction occurs due to the acetone's unavailability in the medium's liquid phase. It was noteworthy that acetalization is an exothermic reaction, with no need for further temperature for glycerol acetalization [138].

6.6.2. Influence of reaction time

The conversion of glycerol and solketal yield was also affected by the duration of the reaction. The optimization of the reaction time for glycerol to solketal is illustrated in Figure 6.11 (b). It was found that as the reaction time increased from 30 min. to 120 min., the percentage conversion of glycerol increased from 44 % to 99.3 %. This rise in conversion can be ascribed to the increased number of reacting species (glycerol and acetone), which aid in forming new bonds following the cleavage of existing ones. However, beyond 120 min. spent on reaction time, the conversion of glycerol decreased. This reduction in glycerol conversion may be attributed to the hydrolysis of the synthesized product, facilitated by water forming during the acetalization process.[134]

6.6.3. influence of catalyst weight percentage

The acetalization reaction for solketal synthesis is highly influenced by the catalyst

loading percentage of SZZ, and the obtained glycerol conversion and solketal yield are depicted in Figure 6.11 (c). In the absence of a catalyst, no glycerol conversion was detected. However, with an increase of the catalyst loading percentage (based on glycerol weight) from 0.5 to 3.0 wt.%, there was a gradual increase in conversion of glycerol from 61 % to 99 %, respectively. This increase can be accredited to the increased availability of the active sites on the catalyst's surface, thereby facilitating the interaction and collision between the acetone and glycerol molecules. Additionally, with an extension in loading of catalyst from 5 wt. %, both glycerol conversion and solketal yield began to decrease, potentially due to the hydrolysis of the synthesized solketal [158].

6.6.4. Influence of ratio of acetone to glycerol reactants

The acetalization reaction of acetone with glycerol is reversible. A higher reactant concentration is necessary to drive the equilibrium towards the product side. In this process, when the glycerol to acetone molar ratio was set at 1:2, the conversion of glycerol was notably very low (i.e., 51 %). However, a further increase in the reactant molar ratio from 1:4 to 1:10 showed a remarkable improvement in conversion and was found to be 99.3 % in Figure 6.11 (d). Further rise of reactant molar ratio (above 1:10), a marginal variation was observed in glycerol conversion. This result could be attributed to the glycerol in acetone's increased accessibility that helps shift the equilibrium toward the product formation side. These outcomes suggest minimal changes were found in glycerol conversion with the augmentation of the reactant molar ratio (i.e., acetone and glycerol) [103].

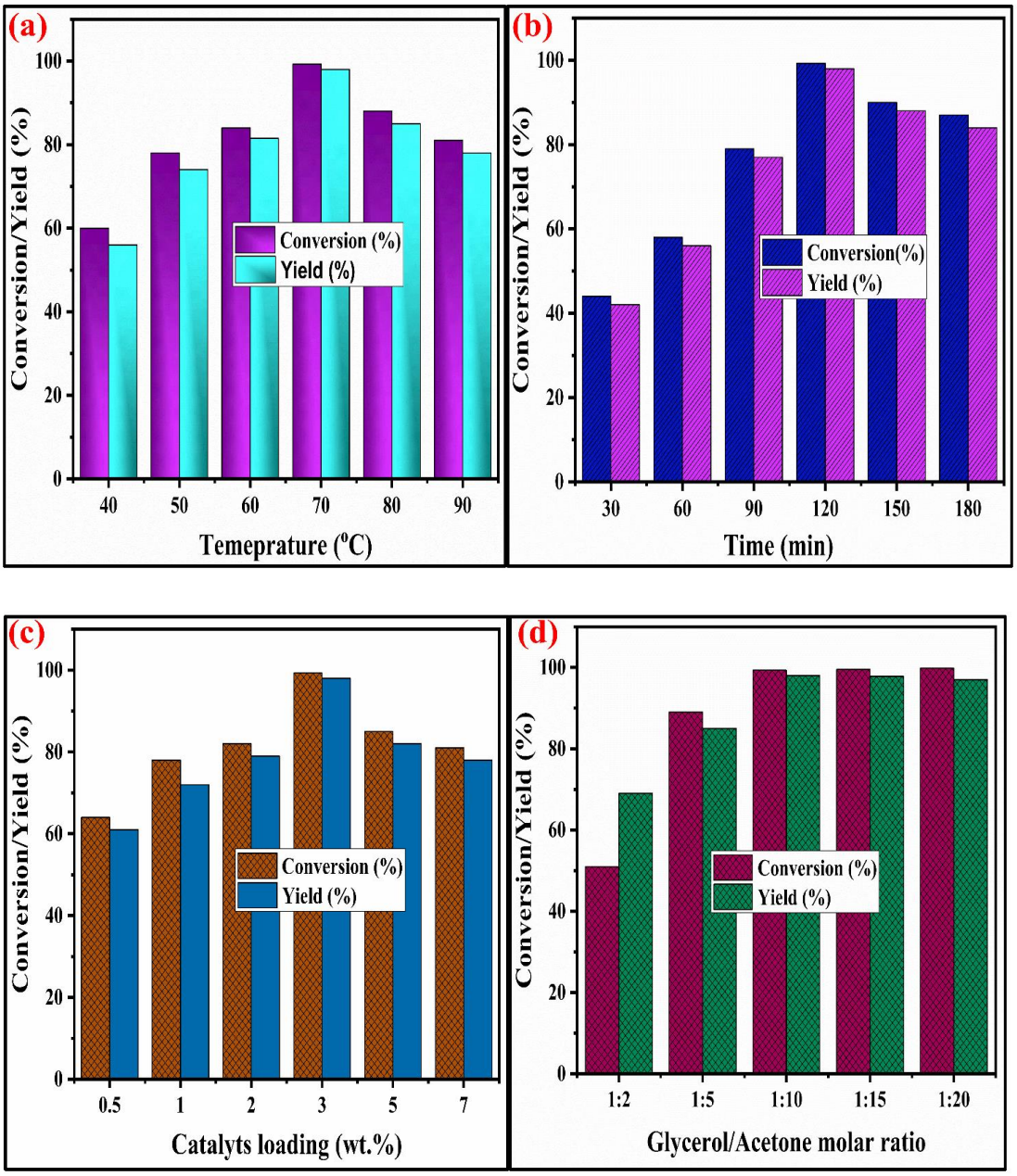

Figure 6.11. Optimization of (a) reaction temperature (glycerol to acetone 1:10 molar ratio, catalyst wt. % = 3, time=120 min.), (b) reaction time (glycerol to acetone=1:10 molar ratio, catalyst wt. % = 3, reaction temperature = 70 °C), (c) catalyst weight percentage (glycerol to acetone 1:10 molar ratio, time=120 min. reaction temperature = 70 °C), (d) Glycerol to acetone molar ratio (reaction temperature = 70 °C, catalyst wt. % = 3, time=120 min.)

6.7. Green metrics studies in glycerol acetalization

As per the postulates of green chemistry, minimizing waste generation in chemical reactions signifies a more environmentally friendly process. As a result, a sustainable process should generate less amount of waste. Therefore, investigating waste generation during the catalytic cycle was important to ascertain the process's overall environmental impact and eco-friendliness. The degree of 'greenness' of the acetalization reaction catalyzed using SZZ catalyst was assessed by considering various key green parameters. These parameters, environmental factor, process mass index, and atom economy, were calculated using the provided equations.

$$\text{E-factor} = \frac{Mass\ of\ the\ produced\ waste\ (g)}{Mass\ of\ the\ desired\ product\ (g)} \quad (6.2)$$

$$\text{Process Mass Index (PMI)} = \frac{Total\ mass\ used\ in\ acetalization\ process\ (g)}{Mass\ of\ product\ \ (g)} \quad (6.3)$$

$$\text{Atom Economy (AE)} = \frac{Mass\ of\ the\ isolated\ product}{Total\ mass\ of\ all\ the\ substance\ produced} \quad (6.4)$$

The E-studies serve as an indicator of the environmental compatibility of the solketal synthesis. A lower E-value reflects the lower waste production during the process. Similarly, PMI is defined as the ratio of total mass of the reactant employed in the acetalization process to the mass of the resultant isolated product. Atom economy, on the other hand, defines the mass of the isolated product relative to the total mass of all the products produced in the synthesis process. The only water as a byproduct generated is benign and serves as a solvent in numerous chemical processes. Similarly, excess acetone was recovered by the rotatory evaporator and further used in the acetalization process. Notably, the reusability of the catalyst and solvent is not considered in the green metrics

calculation. E-factor, PMI, and atom economy were calculated to be 0.81, 1.82 g-1, and 100 %, respectively, demonstrating a minimum waste generation during the glycerol acetalization process [159].

6.8 Reusability study of the catalyst

Catalyst reusability plays a significant role in the acetalization reaction of solketal synthesis. The activity and reusability of the catalyst were studied by performing the batch reaction, and it was found that the catalyst can be used for up to the 5^{th} catalytic cycle. Throughout the repeated cycle, both the conversion percentage and solketal yield remain unaffected, as shown in Figure 6.12. However, beyond the 6^{th} catalytic cycle, a sudden decline in glycerol conversion and solketal yield was observed. The observed catalytic activity loss could be due to some mass loss of sulfur content or pore blockage and surface poisoning by glycerol and acetone during the recycling process. To ascertain the cause of catalyst deactivation, a leaching test was conducted using the hot filtration technique. After a 90 min. reaction period, the catalyst was segregated from the reaction mixture by filtration under hot conditions, during which the glycerol conversion was found to be > 90 %. Subsequently, the reaction was prolonged without the catalyst for an additional 180 min. of the reaction showed a slight increase in glycerol conversion Figure 6.13. This examination demonstrated that the filtrate did not contain a significant amount of soluble active catalyst. Consequently, it demonstrated the catalyst's heterogeneous nature. The XRD and FTIR study of the recycled catalyst is presented in Figure 6.14 (a) & (b). Similarly, the SEM image of the 5^{th} recycled catalyst is displayed in Figure 6.14 (c). The similarity in the plots and image of the reused catalyst with the fresh catalyst validates its catalytic stability.

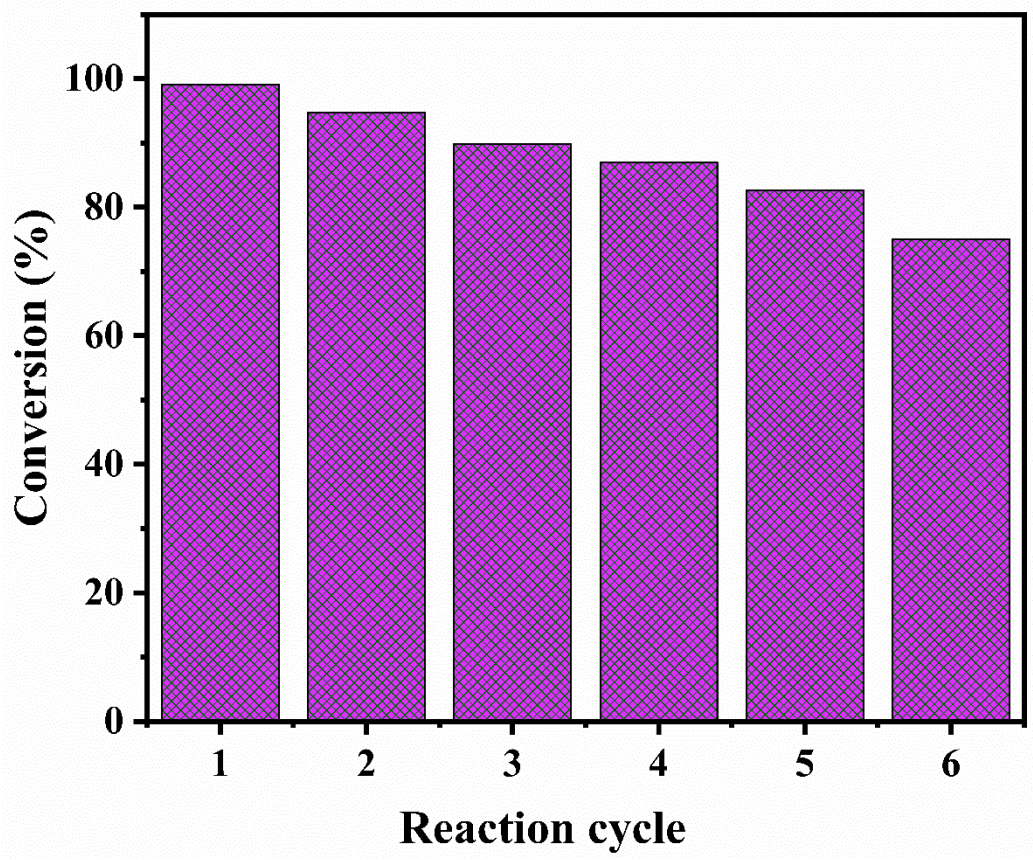

Figure 6.12 Reusability of synthesized SZZ catalyst in solketal synthesis

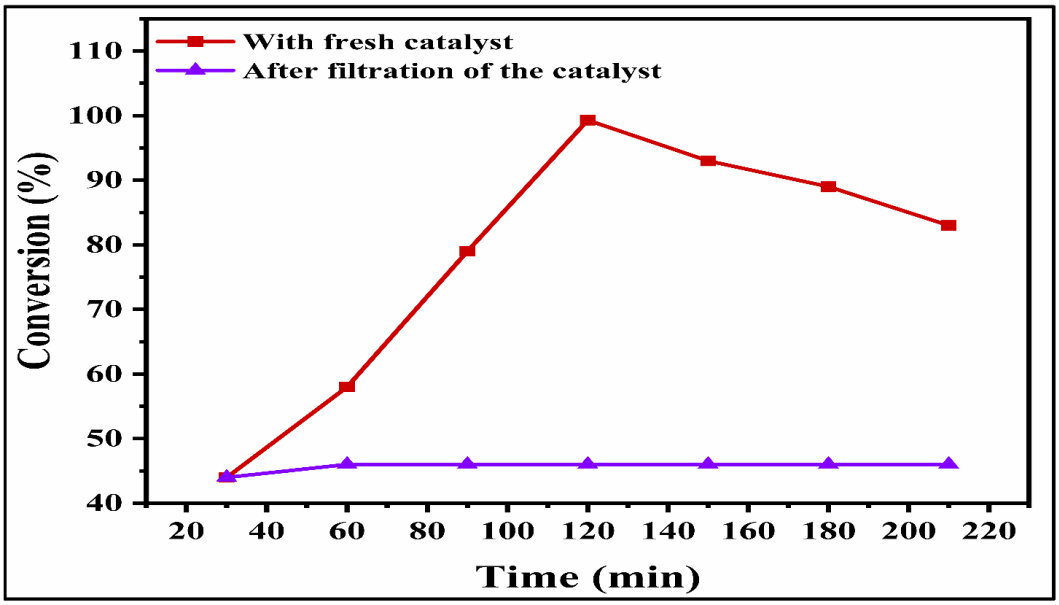

Figure 6.13 Heterogeneity of SZZ catalyst

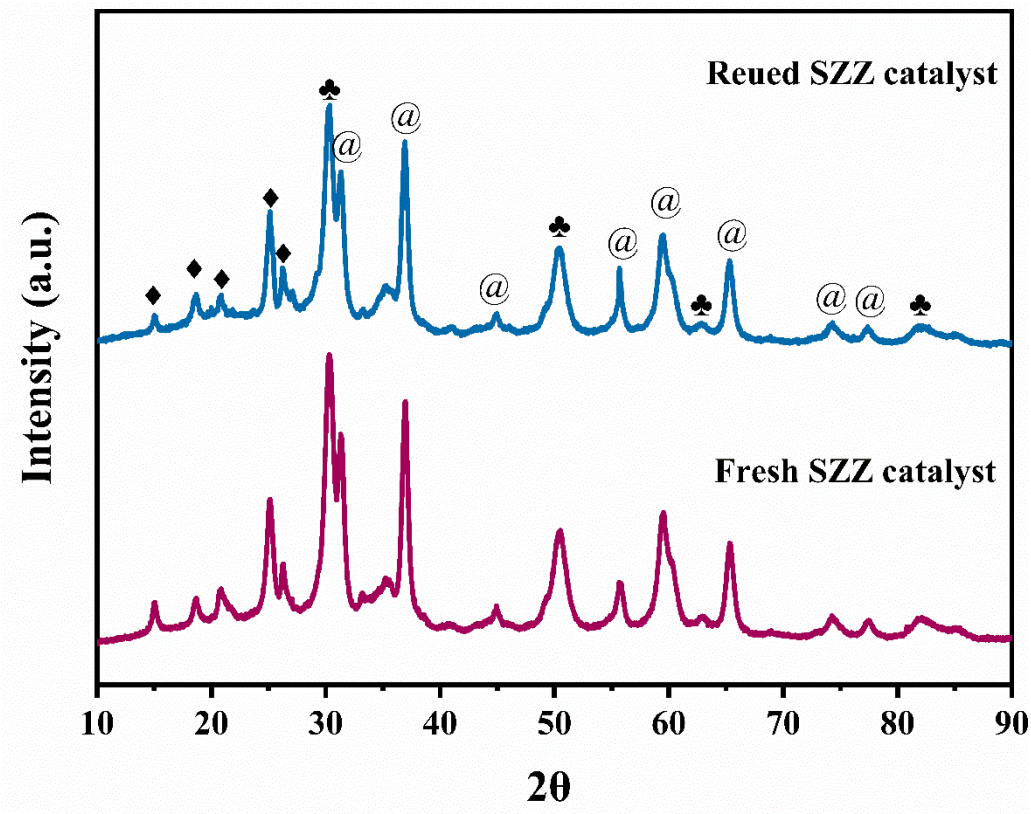

Figure 6.14 (a) XRD image of reused SZZ catalyst

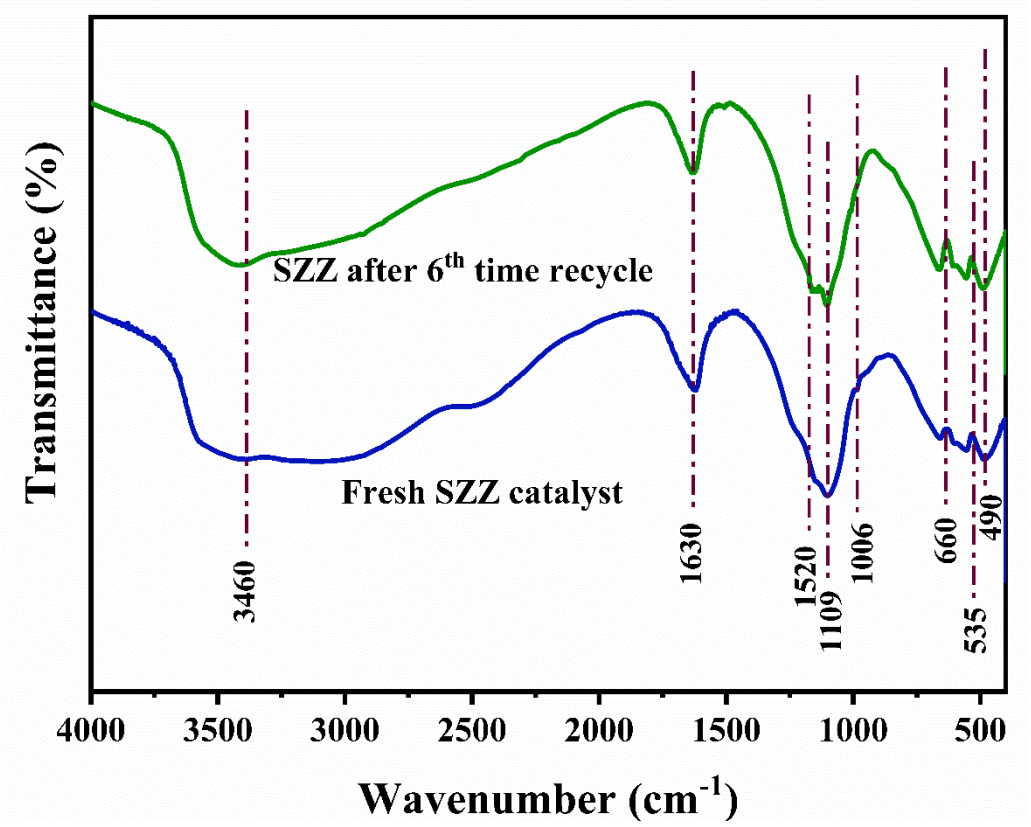

Figure 6.14 (b) FTIR spectra of reused catalyst

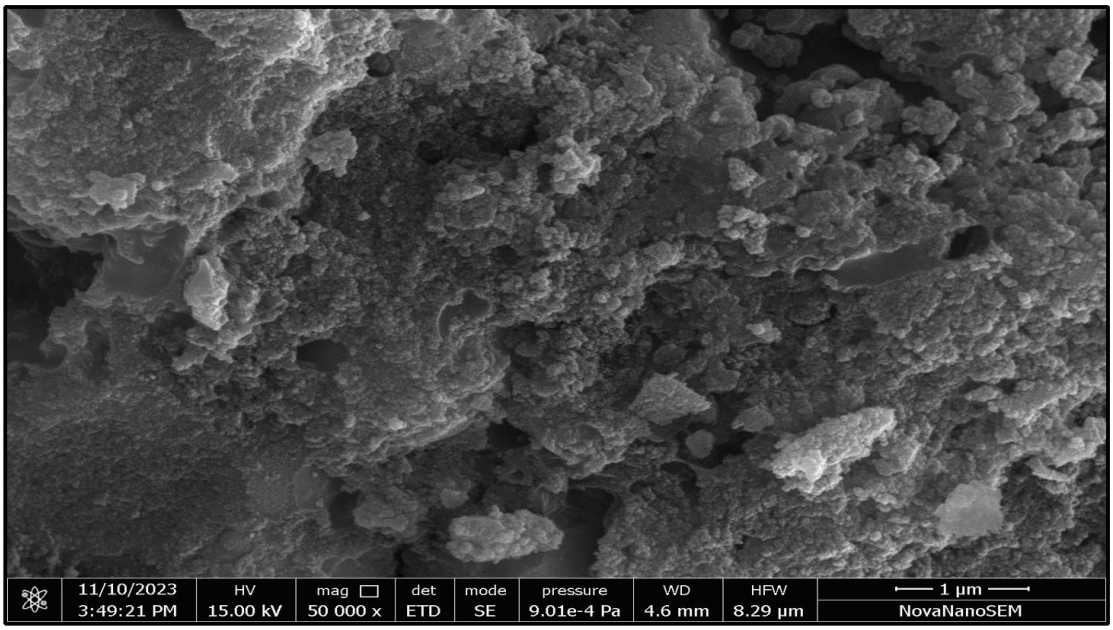

Figure 6.14 (c) SEM image of reused SZZ catalyst

6.9 Comparative study

The heterogeneous acid catalysts for glycerol acetalization under various reaction conditions that have been reported by several studies are tabulated in Table 6.3. Catalysts like P-25, Amberlyst-15 [160], and SO_4^{2-}/CeO_2-ZrO_2 [161] showed an appreciable glycerol conversion, but the time duration for solketal synthesis is very high. In contrast, SZZ catalyst showed good catalytic activity and gave 99.3 % glycerol conversion at 120 min. Similarly, Fe $(NO_3)_3.9H_2O$ showed a good conversion under moderate reaction conditions. Still, it required a higher amount of acetone (i.e., 1:20 M of glycerol and acetone) and is reusable only up to the 3rd reaction cycle [55]. In contrast, the SZZ catalyst utilizes a lower glycerol-to-acetone molar ratio (1:10) and shows excellent catalytic stability till the 5th reaction cycle. Likewise, MoM_3/SiO_2 [59] and Montmorillonite [60] catalysts showed very poor catalytic activity and used solvents like Toluene and CH_3CN and gave low conversion of glycerol. Here, the synthesized catalyst exhibited notable catalytic activity in the solketal synthesis under solvent-free conditions. In this, the

synthesized catalyst is facile and more efficient for the acetalization process. A comparative analysis indicates that the SZZ catalyst exhibits outstanding catalytic activity throughout the reaction when compared to the reported catalysts. The catalyst's thermal stability and reusability established it as an effective heterogeneous acid catalyst for its broad potential applications.

Table 6.3. Comparative study of catalytic activity of synthesized SZZ catalyst with the reported catalyst employed in solketal synthesis

Catalyst	Catalyst loading	Reaction time (min.)	Reaction temperature (^oC)	Gly: Ace molar ratio	Solvent	Glycerol conversion (%)	Endurance capacity	Ref.
20 % MoO_3-ZrO_2	0.03 (gm)	10	50	1:8	free	89	5^{th} reaction cycle	[2]
MOF-808-SO4 (DF) defective/sulfonated	0.01 (gm)	30	78	1:7	free	78	4^{th} reaction cycle	[4]
GS-SO_3H	5 (wt. %)	240	RT	1:4	free	91	5^{th} reaction cycle	[61]
SO_4^{2-}/SnO_2	5 (wt. %)	240	RT	1:1	free	95	5^{th} reaction cycle	[62]
Zr-S	0.3 (wt. %)	60	40	1:6	free	80	4^{th} reaction cycle	[63]
SO_4^{2-}/CeO_2-ZrO_2	9 (wt. %)	480	100	1:3 (benzaldehyde)	Toluene	91.8	Not reported	[57]
Acidic Carbon	3 (wt. %)	60	100	1:2	free	82	5^{th} reaction cycle	[64]
$Fe(NO_3)_3.9H_2O$	0.3 (mol %)	60	25	1:20	free	90	3^{th} reaction cycle	[58]
Zr-S-400	0.6	60	40	1:6	free	80	4^{th}	[6

	(wt. %)						reaction cycle	3]
PSF/K-SiO_2	5 (wt. %)	90	25	1:10	free	86.3	5th reaction cycle	[65]
MoM_3/SiO_2	10 (wt. %)	480	100	1:1(benzaldehyde)	Toluene	72	Not reported	[59]
Montmorillonite	0.7 (wt. %)	30	50	1:4.1	Free	54	3rd reaction cycle	[60]
Montmorillonite	0.7 (wt. %)	30	50	1:4.1	CH_3CN	94	3rd reaction cycle	[60]
DT-851 sulfonic acid resin	5 (wt. %)	120	58	1:20	free	95	10th reaction cycle	[66]
P-25	0.8 (wt. %)	1440	30	1:13	free	87	Not reported	[56]
Amberlyst-15	0.8 (wt. %)	1440	30	1:13	Free	64	Not reported	[56]
SZZ (present work)	3.0 (wt. %)	120	70	1:10	free	99.3	6th reaction cycle	

7. Conclusion

This study provides a more environment-friendly route to produce solketal by using the byproduct glycerol obtained from biodiesel plants in our lab via a transesterification process. We successfully synthesized a heterogeneous acid SZT and SZZ catalyst and

examined their catalytic performance in glycerol acetalization reaction. A comparative study between SZT and SZZ catalysts was performed for solketal synthesis. Several characterization processes like SEM-EDX, XRD, FTIR, TGA, BET-surface area, XPS, and the Boehm titration method revealed sulfur impregnation on the catalyst's surface. All characterizations consistently demonstrated that SZZ catalyst exhibits higher catalytic activity than SZT catalyst. The catalyst's heightened activity relies on its elevated acidity, which is a pivotal factor in gaining a substantial percentage of solketal. The higher acidity of SZZ catalyst was very helpful for the acetalization reaction of glycerol to solketal. The solketal produced underwent quantitative and qualitative analysis through techniques including ^{1}H and ^{13}C NMR, FTIR spectroscopy, and gas chromatography process. The acidity of the synthesized catalyst and the conditions of the reaction played a significant role in influencing both the conversion of glycerol and solketal yield. The higher TOF of the SZZ catalyst makes it more commendable for its catalytic activity than the SZT catalyst. To obtain an excellent solketal yield, optimal reaction conditions were optimized. Greenness parameters like E-factor, PMI, and AE were employed to show that the synthesis route is environmentally benign and eco-friendly in nature. In summary, SZZ catalyst proves to be a cost-effective and highly active catalyst, and reusability is demonstrated up to the 5^{th} catalytic cycle. The repeated utilization of the SZZ catalyst in solketal synthesis enhances the economic feasibility of the process on an industrial level, and the cost-effectiveness nature recognizes the sustainability of the solketal market.